Preparation of Platinum/Carbon Aerogel Nanocomposites Using a Supercritical Deposition Method

Carl D. Saquing,[†] Tai-Tsui Cheng,[‡,§] Mark Aindow,[‡] and Can Erkey*[,†]

Environmental Engineering Program, Department of Chemical Engineering, and Department of Metallurgy and Materials Engineering, Institute of Materials Science, University of Connecticut, Storrs, Connecticut 06269-3136

Received: February 2, 2004; In Final Form: April 5, 2004

Platinum/carbon aerogel (Pt/CA) nanocomposites were synthesized using a supercritical deposition method. Dimethyl(1,5-cyclooctadiene)platinum (II) ($CODPtMe_2$) was dissolved in supercritical CO_2 ($scCO_2$) and impregnated into porous organic and carbon aerogels. The impregnated aerogels were converted to Pt/CA composites by heat treatment ranging from 300 to 1000 °C in the presence of nitrogen gas. Both conventional and high-resolution TEM micrographs showed a good distribution of fairly monodisperse Pt particles throughout the bulk of all the aerogel supports used. The nature and crystallinity of the particles were confirmed using XRD. Increasing the reduction temperature increased both the crystal size and the polydispersity. Crystallite sizes as small as 1 nm were obtained at low reduction temperatures and the particles were single-crystalline. Particle sizes obtained from H_2 and CO chemisorption measurements are consistent with those measured from TEM images, indicating the accessibility of the surface of platinum crystallites. The adsorption isotherm for the $scCO_2-CODPtMe_2-CA$ system was measured at 28 MPa and 80 °C and indicated a strong substrate-precursor interaction which was also corroborated by thermogravimetric analyses (TGA). The isotherms also showed that Pt loadings as high as 40 wt % could be achieved. The results of this study demonstrated that in SCF deposition, it is possible to control the dispersion of metal crystallites on various supports through the strength of the interactions between metal precursors and the substrate and the reduction temperature.

Introduction

Carbon aerogels (CAs) are a relatively new class of engineered carbons.[1,2] They are prepared by pyrolysis of organic aerogels that are synthesized by supercritical drying of the gels obtained by the sol−gel polycondensation reaction of resorcinol and formaldehyde in aqueous solutions. CAs consist of interconnected nanometer-sized carbon particles (3−30 nm) with small interstitial pores (<50 nm) and have high surface areas (400−1500 m^2/g) and very sharp pore size distributions. They are electrically conductive, in contrast to all other types of organic and inorganic aerogels (such as silica aerogels), which are generally insulating materials, and they can be produced as monoliths, thin films, powders, or microspheres.[3,4] They are attractive materials since their microstructure and physical properties can be tuned at the nanometer scale by varying the processing parameters in the sol−gel polymerization, gelation, curing, and pyrolysis steps.[5] As a result, CAs have been investigated for a wide variety of applications including supercharged capacitors,[6] broadband nonreflective materials,[7] materials for electrosorption of ions from aqueous solutions,[8] and adsorbents for removal of organosulfur compounds from diesel.[9]

The high electrical conductivity of CAs coupled with their adjustable pore volume and pore size has promoted research in functionalizing carbon aerogels with platinum for use as an electrocatalyst for fuel cells.[10,11] Such materials may also be an attractive alternative to carbon-supported platinum catalysts used in oxidation and hydrogenation reactions.[12−14] For these applications, minimization of particle size is critical from an economic point of view since Pt is an expensive metal. In their pioneering study, Mayer et al.[11] prepared platinum/carbon aerogel (Pt/CA) composites by adding commercially available platinum black (200−500 nm particle size) to the sol after dispersing it ultrasonically in an aqueous solution. Since the average size of the platinum crystallites in such a composite would be at least that of the platinum black particles, they suggested using platinum colloids to decrease the crystallite size. Pajonk et al.[15] described a new method to synthesize Pt/CA composites. RF aerogels were prepared by perchloric-acid-catalyzed polymerization in acetone instead of water. After curing and supercritical extraction of acetone, the samples were pyrolyzed. The samples were impregnated with H_2PtCl_6 in acetone, whereby acetone was supercritically extracted and the sample was calcined and reduced with hydrogen. The dispersion of platinum was 23% and the platinum content was 0.44 wt %. Unlike standard CAs, the materials were macroporous. Maldonado-Hodar et al.[16] reported on the textural characterization of Pt/CA composites prepared using a water soluble platinum salt, $Pt(NH_3)_4Cl_2$, instead of Na_2CO_3 as the polymerization catalyst. After curing, water was exchanged with acetone and acetone was extracted by supercritical carbon dioxide. Subsequently, the platinum-containing organic aerogels were pyrolyzed in flowing nitrogen and activated by steam or CO_2. The resulting Pt/CA composites had a Pt content of 0.5 wt % and high mesopore and very high macropore volumes. The authors did not provide any data on dispersion and crystallite size. The major disadvantage of such a method is the interference of the

* Corresponding author.
[†] Department of Chemical Engineering.
[‡] Department of Metallurgy and Materials Engineering.
[§] Present address: Engine Controls Systems, Hamilton Sunstrand, One Hamilton Road, M/S B2-2-MGG24, Windsor Locks, CT 06096-1010.

10.1021/jp049535v CCC: $27.50
Published on Web 05/12/2004

TABLE 1: Summary of Studies Made by Watkins et al. and Morley et al. on the Deposition of Metals into Solid Substrates by SCF

substrate	precursor[a]	contact conditions	contact time (h)	precursor reduction	average particle size (nm)	particle size range
silicon wafer[b]	$CODPtMe_2$	80 °C and 155 bar	2	H_2 in $scCO_2$ at 80 °C and 155 bar	90†	80−100
poly(tetrafluoroethylene) (PTFE)[b]	$CODPtMe_2$	80 °C and 155 bar	4	H_2 in $scCO_2$ at 80 °C and 155 bar	65†	30−100
anopore aluminum oxide membrane[b]	$CODPtMe_2$	80 °C and 155 bar	4	H_2 in $scCO_2$ at 80 °C and 155 bar	65†	30−100
poly(styrene-divinylbenzene)[c]	Ag(hfpd)tetraamine	40 °C and 272 bar	24	H_2 at 60°C and 68 bar	34	0−200
poly(styrene-divinylbenzene)[c]	Ag(hfpd)tetraglyme	40 °C and 272 bar	24	H_2 at 60°C and 68 bar	42	0−200
silica aerogel[c]	Ag(hfpd)tetraamine	40 °C and 272 bar	24	H_2 at 60°C and 68 bar	23	0−200
silica aerogel[c]	Ag(hfpd)tetraglyme	40 °C and 272 bar	24	H_2 at 60°C and 68 bar	42	0−200

[a] COD = 1,5 cyclooctadiene; Me = methyl; hfac = hexafluroroaceylacetonate; hfpd = 1,1,1,5,5,5-hexafluoropentane-2,4-dione. [b] Watkins et al. [c] Morley et al. [d] Average calculated from the range values.

precursors with polymerization chemistry resulting in fragile materials.[17] Glora et al.[10] and Hammerschmidt et al.[18] employed sputtering and plasma deposition processes in the application of a thin layer of platinum to the carbon aerogel. Particle sizes obtained from sputtering ranged from 20 to 30 nm, while no data on Pt crystallite size or dispersion were reported from the plasma method.

In this work, we investigated the applicability of a supercritical fluid (SCF) deposition method to prepare Pt/CA composites with a high dispersion of platinum. An SCF exhibits an attractive combination of the solvent properties of a gas and a liquid. Its gas-like diffusivity and viscosity favor rapid diffusion and permeation, while its liquid-like density allows for dissolution of a wide range of organometallic precursors. Moreover, the low surface tension of an SCF permits good penetration and wetting of ultrafine pores which are usually not accessible to liquid solvents. Another distinct advantage of an SCF is the dramatic sensitivity of its density to changes in temperature and/or pressure; hence its solvent properties can be manipulated easily during processing. Among the SCFs, supercritical carbon dioxide is particularly attractive since it is environmentally friendly and safe because of its low toxicity, low reactivity and nonflammability. CO_2 leaves no residue in the processed product because of its gaseous character near ambient conditions. Moreover, Machek et al.[19] showed that the distribution of a metal such as Pt on the carbon support surface depends on the solvent used for deposition. Since carbon is essentially hydrophobic in nature, CO_2 having a nonpolar character should readily penetrate to the interior of the porous CA, which should lead to a more uniform distribution throughout the material.

SCF deposition involves the dissolution of an organometallic precursor in a supercritical fluid and the exposure of the substrate to this solution. After impregnation of the substrate with the precursor, the precursor−substrate composite can be converted to metal−substrate composite by (1) depressurization of the supercritical solution and subjecting the precursor−substrate composite to hydrogen or heat treatment or (2) injecting of a reducing agent such as hydrogen into the supercritical solution. The first method was used by Morley et al.[20] to produce silver particles within porous substrates of poly(styrene-divinylbenzene) beads and silica aerogels. The second method was used by Watkins et al.[21,22] to form metallic films of platinum on solid substrates including silicon wafers and polymers. The results from these studies are summarized in Table 1 and, generally, they indicate a high degree of aggregation, resulting in large crystallite sizes and a wide distribution of particle sizes. Particle formation and growth in these two studies occur by three different mechanisms. In the first method, the adsorbed precursors are converted to their metal form and the growth of particles is controlled by surface diffusion of the metal atoms and/or precursor molecules. In the second method, an additional mechanism contributes to particle formation and growth. When hydrogen is injected into the supercritical carbon dioxide−precursor solution, hydrogen reacts with the adsorbed precursor molecules at the surface. The resulting platinum particles at the surface continue to grow, because they act as catalysts for reaction of hydrogen and precursor at the surface.[23−25] The particle growth continues until the entire metal precursor or hydrogen in the $scCO_2$ phase is consumed. In this method, it is also possible that hydrogen and the precursor react in the supercritical phase and the resulting platinum particles precipitate at the surface of the substrate. If there is a strong interaction between the substrate and the precursor, it may be possible to prepare metal particles with narrow size distributions and with sizes that are significantly lower than the studies reported in the literature.

In this study, we demonstrate that nanosized platinum crystals with particle sizes ranging from 1 to 4 nm with a very narrow particle size distribution can be incorporated into high surface area nanoporous resorcinol−formaldehyde aerogels (RFAs) and CAs via SCF deposition followed by thermal reduction at atmospheric pressure. We also report our results on the equilibrium adsorption of the SCF−metal precursor−substrate system at the impregnation conditions. These data provide an understanding of the interaction between the components involved and how the metal precursor partitions between the SCF and substrate. Moreover, the data also establish the amount of metal that can be incorporated into the substrate. The materials were characterized by H_2 and CO chemisorption, nitrogen adsorption, X-ray diffraction (XRD) and transmission electron microscopy (TEM).

Experimental Section

Materials. The following chemicals were obtained from Aldrich and used without further purification: resorcinol (99%), formaldehyde (37%), sodium carbonate (99.99%). Dimethyl-(cyclooctadiene)platinum (II) (99.9%) was obtained from STREM. Carbon dioxide (research grade 4.8, 99.998%) and nitrogen (prepurified grade 4.8, 99.998%) were purchased from Airgas. Water was deionized and distilled.

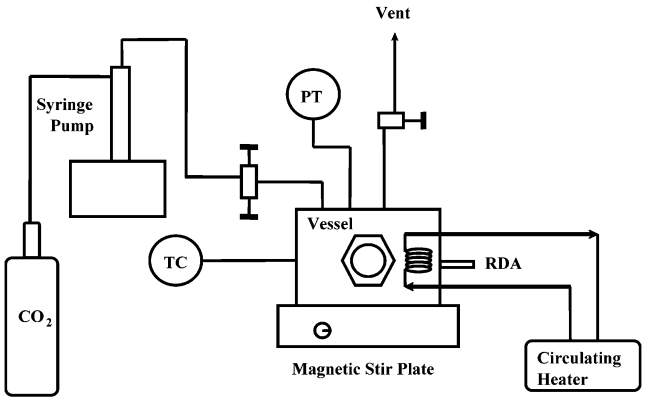

Figure 1. Schematic diagram of the apparatus used for supercritical drying.

Apparatus and Procedure. Resorcinol−formaldehyde aerogels (RFAs) and CAs were prepared by polymerization of resorcinol with formaldehyde in water based on the procedures of Pekala.[1] In a typical procedure, a tube containing resorcinol, formaldehyde, sodium carbonate, and water at appropriate concentrations was kept at room temperature for 1 day, at 50 °C for another day, and at 90 °C for 3 days in a Blue M Stabil-Therm gravity oven. At the end of the three-day period, the monolith was taken out of the test tube and immersed in approximately 200 mL acetone where it was kept for a period of at least 12 h. Subsequently, acetone was supercritically extracted, resulting in RFA. The RFA was converted to CA by pyrolysis in an inert nitrogen atmosphere. In the pyrolysis process, an RFA monolith was placed in an alumina process tube (Cole-Parmer) with dimensions of 25 mm (ID) × 28 mm (OD) × 1219.2 mm (L). The tube was inserted into a tube furnace (model F1125 Thermolyne) and heated under flowing nitrogen gas at 100 cm^3/min. The oven was kept at this temperature for another six (6) hours. After cooling to room temperature, the CA monolith was removed from the tube. Two CAs with different pore sizes were prepared by varying the resorcinol and formaldehyde-to-water ratio. The Brunauer, Emmett, and Teller (BET) surface area (SA) and pore size distribution of RFAs and CAs were obtained from at least ninety-point nitrogen adsorption/desorption analyses using a Micromeritics ASAP 2010 instrument. The CA and RFA samples were outgassed at 200 °C and 120 °C, respectively. The lower outgassing temperature for RFAs ensured that thermal decomposition was prevented. BET SA was calculated from the linear portion of the BET equation over the relative pressure range of 0.03 to 0.3. Pore size distributions were derived from the Barrett, Joyner, and Halenda (BJH) method, as provided by the Micromeritics ASAP 2010 instrument.

A schematic diagram of the apparatus utilized for the supercritical deposition step is shown in Figure 1. In the deposition step, a certain amount of a monolithic aerogel (either RFA or CA), together with a certain amount of $CODPtMe_2$, was placed in a high-pressure vessel (internal volume of 54 cm^3), custom manufactured from 316 stainless steel and equipped with two sapphire windows (diameter = 32 mm, thickness = 12 mm), sealed on both sides with PEEK seals. The vessel was heated to 80 °C and charged with carbon dioxide to 27.7 MPa using a syringe pump (ISCO, 260D) and was kept at this condition for 24 h to ensure that adsorption equilibrium was reached. The adsorption equilibrium time of 24 h was established after comparing it to an equilibration time of 48 h. The metal loadings obtained using the two adsorption times agreed within ±1% (10.2 wt % (24 h); 10.1 wt % (48 h)). Subsequently, the vessel was depressurized and the monolith was taken out of the vessel. The precursor-loaded monolith was placed in a quartz tube (GE), inserted into a tube furnace (model F1125 Thermolyne tube furnace), and heated under flowing nitrogen gas at 100 cm^3/min. During this process, the precursor was converted to the base metal. The Pt/CA composite was weighed using an Ohaus analytical balance (Adventure model AR2140) accurate to ±0.1 mg. The amount of platinum deposited (metal loading) was determined from the weight gain of the precursor-loaded sample. When RFAs were used as the substrates, heating also resulted in their transformation to CAs. For a representative selection of the Pt/CA composites produced, hydrogen, and CO chemisorption measurements (Micromeritics ASAP 2010) and transmission electron microscope (TEM) analyses were performed. For H_2 and CO chemisorption, all samples were subjected to a series of evacuation steps prior to analysis at 35 °C. This involved evacuating the sample at 375 °C for 120 min followed by another evacuation step at 35 °C. Equilibration time at a certain pressure was determined for all the samples analyzed and varied from 35 min to an hour. The adsorption stoichiometry was assumed to be dissociative, which corresponds to a stoichiometric factor of 2. The amount of hydrogen adsorbed dissociatively to platinum was obtained from the difference between the total adsorption and the adsorption assigned to both the physisorbed species in the support and the weakly chemisorbed species in the metal. These were deduced by extrapolation to zero pressure from the isotherms obtained in the first and repeat analyses, respectively.

TABLE 2: Pore Properties of Substrates Used in Supercritical Deposition

substrate	BET SA (m^2/g)	average pore diameter nm BET	average pore diameter nm BJH	pore volume (cm^3/g)
RF6	889	5.6	5.5	1.24
CA4[a]	741	4.1	4.3	0.78
CA20	629	19.3	20.7	3.03

*This carbon aerogel was obtained by pyrolysis of the RF6 precursor.

The samples for TEM were prepared by crushing with a mortar and pestle, and were then suspended in a volatile solvent. A drop of the resulting suspension was deposited onto a holey-carbon coated TEM grid. Conventional bright field TEM images and selected area diffraction patterns were obtained in a Philips EM420T operating at an accelerating voltage of 100 kV. High-resolution phase-contrast lattice images were then obtained in a JEOL 2010 FasTEM equipped with a UHR objective lens polepiece (spherical aberration coefficient $C_s = 0.5$ mm) which gives a point-to-point resolution of 0.18 nm at an accelerating voltage of 200 kV.

The X-ray diffractograms were recorded using a Cu Kα source in a SCINTAG diffractometer (model XDS 2000). The diffractometer was operated in continuous scan mode at a scan rate of 1 degree/minute in the range of 5−90° (2θ).

Thermogravimetric analyses (TGA) were performed using a hi-res TGA 2950 thermogravimetric analyzer (TA Instruments). Ramp rates and nitrogen flowrates were varied from 5 to 20 °C/min and 75−100 cm^3/min, respectively.

Results and Discussion

The pore properties of the aerogel substrates are provided in Table 2. The substrates used in the deposition step are represented by two capital letters with a number, where the letters refer to the type of aerogel (either RF or CA) and the number represents the average pore size in nanometer units. Carbon

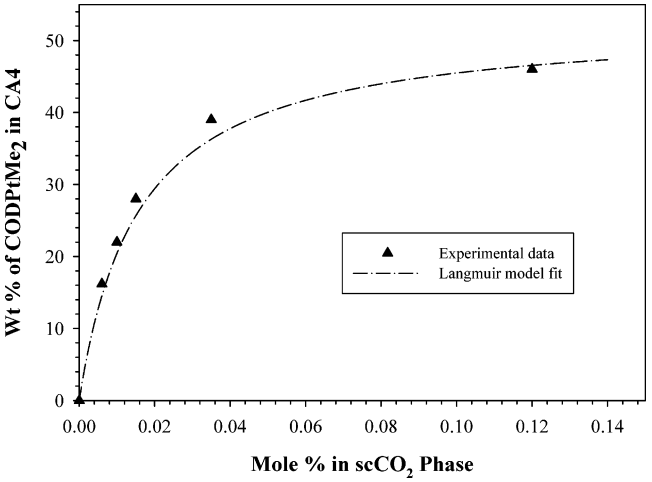

Figure 2. Adsorption isotherm of $CODPtMe_2$ in $scCO_2$ at 80°C and 27.7 MPa.

TABLE 3: Parametric Constants of $CODPtMe_2$ Adsorption Isotherm in $ScCO_2$ According to the Langmuir Model

	Langmuir Isotherm			
adsorbent	R^2	K_l	Q_o	K_l*Q_o
CA4	0.982	61.00	54.64	3333.0

aerogels have lower BET SAs, pore diameters, and pore volumes compared to their RF precursors. When RFAs or CAs were contacted with $CODPtMe_2$ dissolved in $scCO_2$, they adsorbed a substantial amount of $CODPtMe_2$. The adsorption isotherm at 353 K and 27.7 MPa for the system of $CODPtMe_2$, $scCO_2$ and CA4 was obtained and is shown in Figure 2. The adsorption isotherm provides a measure of the partitioning of the Pt precursor between the CA adsorbent and $scCO_2$. The uptakes are high, enabling high platinum loadings. One can control the amount of precursor that can be impregnated, and thus the subsequent metal loading, fairly easily. The isotherm also indicates that there is a limit on how much precursor can be impregnated into the aerogel. The isotherms were fitted to the Langmuir model, which is expressed by the following equation:

$$q = \frac{K_l Q_o C}{1 + K_l C} \quad (1)$$

where K_l is the Langmuir adsorption or adsorption equilibrium constant and is correlated to the heat of adsorption, Q_o is the adsorption capacity, and $K_l Q_o$ is a measure of the relative affinity of the solute toward the surface of the adsorbent. The Langmuir constant for the isotherm is also listed in Table 3. The value of $K_l Q_o$ is high, signifying that $CODPtMe_2$ has more affinity for the adsorbent than for the adsorbate during adsorption in $scCO_2$ solution. This is an indication of a strong interaction between the substrate and the metal precursor.

The heat treatment of $CODPtMe_2$-loaded aerogels resulted in Pt/CA composites. TGA of pure $CODPtMe_2$ and of $CODPtMe_2$-loaded CA4 were performed in N_2. The TGA of the latter in effect simulates the thermal reduction performed in this study and should provide both the temperature range of thermal decomposition and an indication of the extent and dynamics of ligand removal. Figure 3 presents the TGA thermograms obtained in the temperature range of 25 to 600 °C. The majority weight loss occurred between 100 and 200 °C for both pure and impregnated samples; however, the weight loss with pure $CODPtMe_2$ was substantially higher than the expected weight loss of 41% if all of the ligands in the precursor were eliminated

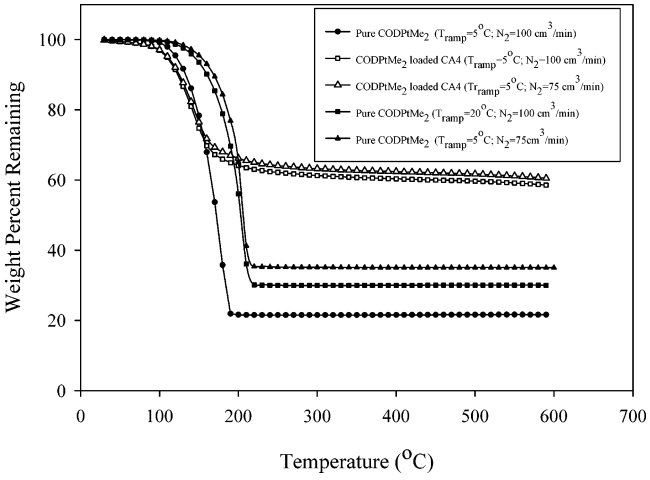

Figure 3. TGA thermograms of pure and adsorbed $CODPtMe_2$ on CA4 at different temperature ramp rates (5−20 °C/min) and nitrogen flow rates (75−100 cm^3/min). The CODPtMe2 loading in CA4 is 40 wt %.

(hereafter referred to as the theoretical weight loss). The higher weight loss is attributed to the volatilization of $CODPtMe_2$ that either precedes or accompanies the decomposition process. When the flow rate of the N_2 gas was increased or the temperature ramp rate was decreased, the weight loss increased which supports the view that the precursor is volatilizing.

On the other hand, in the $CODPtMe_2$-impregnated CA, the weight loss (39−40%) was close to the theoretical value (well within the instrumental precision) at all gas flow rates. This shows that the precursor does not volatilize upon heating when it is in the adsorbed state in the CA matrix, a further indication of the strong interaction between the precursor and the CA matrix. The adsorbed precursor is converted to Pt and the decomposition products are removed completely. This finding was further substantiated by FTIR and acid digestion experiments. FTIR analysis of the Pt/CA composite showed the absence of spectral peaks that correspond to functional groups associated with the ligands. The platinum content of one of the Pt/CA composites was determined by acid digestion. In this experiment, the sample (6.1 wt % Pt content as determined gravimetrically) was digested with a mixture of hydrochloric and nitric acid, and the resulting solution was analyzed by inductively coupled plasma (ICP) spectroscopy for its platinum content. The analysis yielded a value of 5.9 wt % for the platinum content of the composite, which is in good agreement with the content determined gravimetrically. The difference is within 5%, proving that practically all of the ligand is eliminated.

Pyrolysis of impregnated RFAs at 500 °C resulted in Pt/CA composites. Examples of both conventional bright-field and high-resolution TEM micrographs from such samples are shown in Figure 4. These indicate the presence of fairly monodisperse Pt particles with an approximately spherical morphology. When $CODPtMe_2$-impregnated RFAs were pyrolyzed at 1000 °C, there was a dramatic increase in particle size (2−10 nm) and a marked agglomeration of particles as shown in Figure 5. Moreover, there was a distinct broadening of the particle size distribution. The increase in the reduction temperature may have provided more thermal energy to the individual Pt particles, and hence increased their mobility, allowing them to coalesce and form larger entities. In some of these particles, the crystalline structure of the particles is revealed by the presence of lattice fringes. In Figure 5b, for example, continuous lattice fringes across the width of the particles indicate that they are single crystals, and are not multiply twinned or polycrystalline.

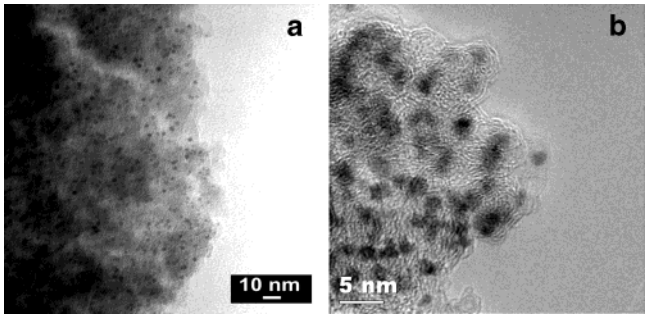

Figure 4. TEM micrographs obtained from sample C30 (20 wt % Pt) reduced/pyrolyzed at 500 °C: (a) conventional bright-field image, (b) high-resolution lattice image.

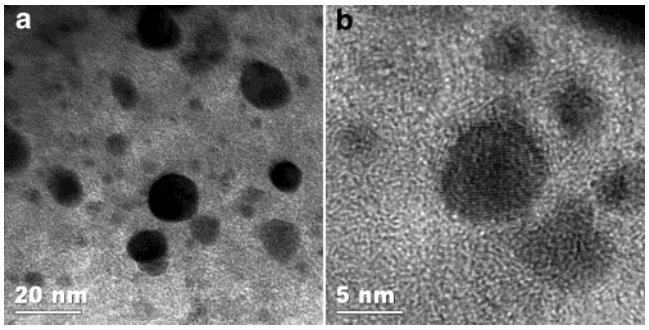

Figure 5. TEM micrographs obtained from sample C32 (20 wt % Pt) reduced/pyrolyzed at 1000 °C: (a) conventional bright-field image, (b) high-resolution lattice image.

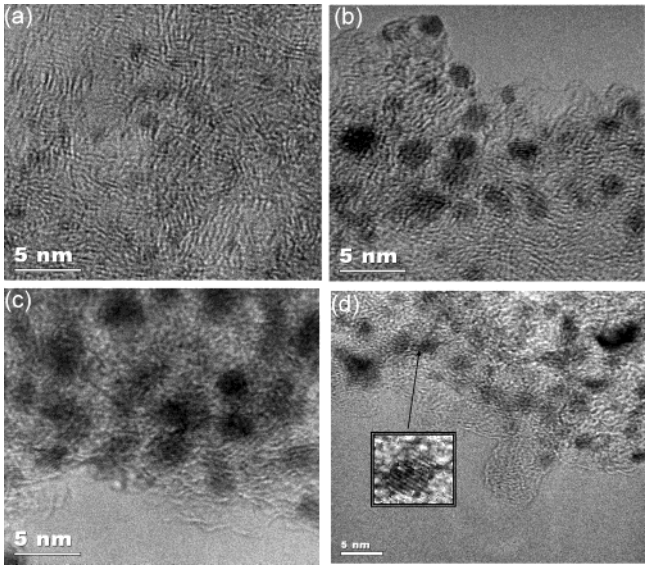

Figure 6. High-resolution TEM micrographs obtained from Pt/CA composites with different Pt loadings: (a) C35 (10 wt %); (b) C45 (20 wt %); (c) C48 (30 wt %); (d) C64 (40 wt %). The support used in 6(a−c) is CA4 while that in 6d is CA20. The inset picture in 6d shows the lattice fringes in a particle.

Alternatively, Pt/CA composites were prepared by heat treatment of $CODPtMe_2$ impregnated CAs. Samples of CAs were prepared with Pt loadings of 10, 20, 30, and 40 wt %. The substrate used for metal loadings from 10 to 30 wt % was CA4 while that at 40 wt % was CA20. Representative TEM images obtained from each of these samples are presented in Figure 6. TEM micrographs taken from a sample using this procedure revealed finely dispersed spherical Pt particles uniformly distributed throughout the bulk, similar to those obtained when RFAs were used as substrate.

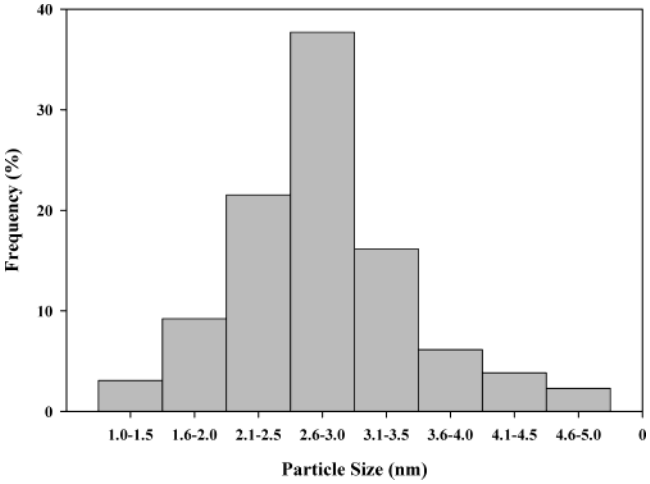

Figure 7. Particle size distribution of the Pt/CA composite C48 (30 wt %).

The particle size distribution of sample C48 (30 wt % Pt) was also obtained by direct measurement of the particle size from several high resolution TEM images. Only regions in sharp focus with a fairly uniform carbon aerogel background were measured, and all of the particles in these regions were counted. In cases where a particle was nonspherical (which was rare), the longer dimension was considered. A total of 130 particles were measured. Figure 7 shows the particle size distribution of C48. The distribution is unimodal, giving an average particle size of 2.8 nm with a standard deviation of 0.7 nm.

Crystallite sizes as small as 1 nm were obtained at a Pt loading of 10 wt %. The main difference between samples with different Pt loading is the packing density of metal clusters observed in each of the images. It is evident that both the size of the particles and the number per unit area increased with increasing metal loading. This is not unexpected since the higher the concentration of Pt atoms, the higher the interaction between them leading to higher incidence of coalescence. Hence, the metal loading may be one parameter that can be manipulated to control particle size. However, it is interesting to note that even though the metal loading was higher for C64 than C48, the particle size was similar. This may be due to the much higher pore volume in CA20 than in CA4. We note that, here again, continuous lattice fringes were observed, indicating that the particles are single crystals: one example is shown in the inset of Figure 6d.

The uniformity of the distribution of platinum crystals within the monolith was verified by taking TEM micrographs from samples corresponding to different locations in the monolith as shown in Figure 8. In all the TEM micrographs obtained, there were no platelets, mirrors, or flakes of the Pt metal observed as reported in the study carried out by Morley et al.[20] They suggested that the platelets or large particles were those that precipitated and agglomerated on the external surface of the substrate when the supercritical solution was depressurized after the impregnation step. In our case, the amount of the precipitate was very small compared to the amount adsorbed within the substrate. The equilibrium concentrations in the fluid phase were very low in the impregnation experiments based on the adsorption isotherm. Furthermore, any small amount that may have precipitated at the surface during depressurization would have volatilized during thermal reduction in flowing nitrogen.

The nature and crystallinity of the deposited Pt particles were further confirmed by the XRD spectra of a representative Pt/CA composite and of a naked CA, and these are shown in Figure 9. The arrows in this figure indicate where the peaks for

TABLE 4: Hydrogen Chemisorption and TEM Results from Pt/CA Composites

sample	substrate	red.[a] temp (°C)	Pt %	platinum surface area (m^2/g metal)	dispersion (%)	crystallite size (nm)	crystallite size from TEM (nm)
C35	CA4	350	10	172.0	69.6	1.6	1.0
C45	CA4	300	20	98.9	40.0	2.8	2.5
C48	CA4	300	30	83.6	33.9	3.3	3.0
C64	CA20	300	40	79.4	32.2	3.5	3.0
C64[c]	CA20	300	40	91.4	37.0	3.1	3.0

[a] Red. = Reduction. [b] Diff. = Difference. [c] From CO chemisorption with assumed stoichiometric factor of 0.7.

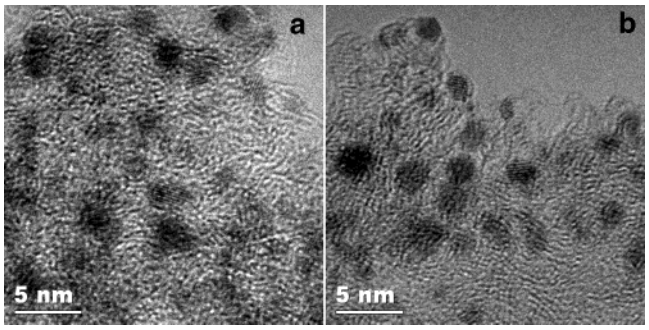

Figure 8. High-resolution TEM micrographs obtained from sample C45 (20 wt % Pt): (a) near the surface of the monolith; (b) near the center of the monolith.

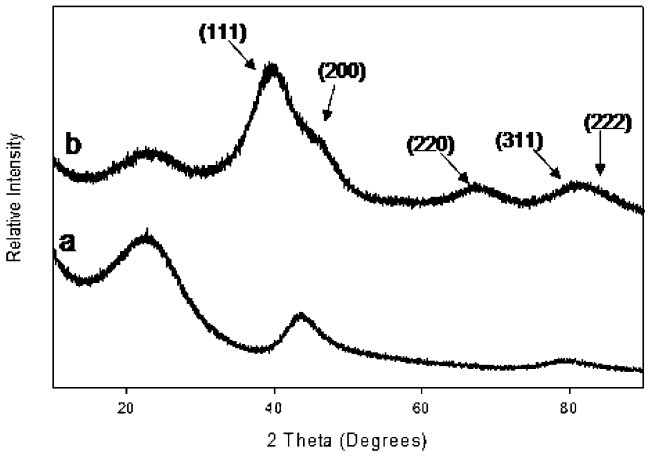

Figure 9. XRD spectra obtained from (a) CA20; (b) Pt/CA composite (C64).

elemental platinum are expected.[26] The peaks in the XRD spectrum of the Pt/CA composite are relatively broad, which is indicative of small crystallite size. The (200) and (222) peaks are not resolved clearly, but this is due to a combination of overlap with adjacent Pt peaks and superposition onto a background consisting of broad peaks from the CA. The XRD spectrum of the CA support has peaks akin to graphitic carbons, indicating a degree of ordering and limited growth of graphitic crystallites.[27] The crystallite size was estimated using Scherrer's formula and the (220) reflection is 2.0 nm, in close agreement with the TEM data.

Crystallite surface area, platinum dispersion, and particle size were determined from chemisorption data using hydrogen as the adsorbate. A typical chemisorption isotherm of a Pt/CA composite along with the isotherm of naked CA is presented in Figure 10. The data show that there is negligible intrinsic adsorption by the naked CA. There is also a large difference in the amount of adsorbed H_2 between the first analysis and repeat analysis of the Pt-loaded CA, which shows that a significant amount of H_2 is adsorbed by weak chemisorption and/or by hydrogen spillover.[28] The chemisorption results are summarized

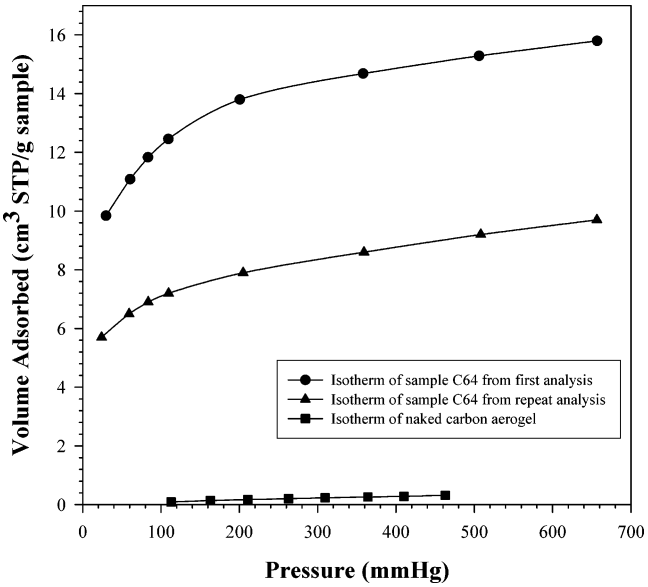

Figure 10. Hydrogen chemisorption isotherms of sample C64 and naked carbon aerogel.

together with the particle sizes measured from the TEM micrographs in Table 4.

Based on hydrogen chemisorption data, platinum dispersions and surface areas ranged from 32 to 70% and 80 to 172 m^2/g Pt, respectively, and decreased with increasing metal loading, except for sample C64. Particle diameters were calculated from chemisorption data using the following equation:

$$S = \frac{6}{\rho_{Pt} d} \tag{2}$$

where S is the Pt surface area, ρ_{Pt} the Pt density, and d the diameter of the particle, which is assumed to be spherical in shape. Comparisons show that particle sizes from H_2 chemisorption concur reasonably well with that measured from TEM images. This suggests that the assumed adsorption stoichiometry is accurate, and it also corroborates the qualitative trend of increasing particle diameter with metal loading discussed previously. One of the samples (C64) was subjected to CO chemisorption. CO is believed not to suffer significantly from the excessive incorporation problem that H_2 exhibits in carbon-supported Pt catalysts.[28] The repeat analysis using CO showed significantly lower physisorption and/or weak chemisorption with the Pt/CA composite. In the literature, the stoichiometric factor for CO was found to vary from 0.7 to 2 (bridged interaction) depending on the nature of CO interaction with platinum. According to Anderson,[28] as the particle diameter becomes small, the stoichiometric factor approaches unity (linear interaction). Moreover, infrared spectroscopy has shown that the most abundant CO species adsorbed with Pt in silica support is the linear type.[29] On the other hand, the use of a stoichiometric factor of 0.7 was found to give good agreement for crystallite

sizes calculated from CO chemisorption data when compared with other independent methods.[30−33] When the stoichiometric factor assumed in this study is 0.7, the particle diameter determined from CO chemisorption is more consistent with diameters determined using TEM and H_2 chemisorption. The agreement between the TEM and chemisorption results strongly suggests that the metallic surface is accessible to small molecules such as H_2 and CO. It should be pointed out though, that particle diameters from chemisorption analysis are consistently higher than those measured using TEM; however, this difference is small.

Conclusions

Platinum/carbon aerogel nanocomposites were synthesized using a supercritical deposition method. $CODPtMe_2$ was dissolved in supercritical CO_2 ($scCO_2$) and impregnated into porous organic and carbon aerogels. The impregnated aerogels were subjected to heat treatment at different temperatures ranging from 300 to 1000 °C in the presence of nitrogen gas, resulting in Pt/CA composites. High Pt loadings ranging from 10 to 40 wt % and crystallite size as small as 1 nm were achieved, and both are believed to be associated with the strong substrate−precursor interaction. Both conventional and high-resolution TEM micrographs showed a good distribution of fairly monodisperse Pt particles throughout the bulk of all the aerogel supports used. The nature and crystallinity of the particles was confirmed from XRD spectra. High-temperature reduction resulted in larger crystallites and increased polydispersity. Particle sizes obtained from H_2 and CO chemisorption measurements are consistent with those measured from TEM images, indicating the accessibility of the surface of platinum crystallites.

The adsorption isotherm for the $scCO_2-CODPtMe_2$−CA4 system at the SCF impregnation conditions was measured and indicated a strong substrate−precursor interaction, which was also corroborated by TGA data. The results of this study demonstrate that SCF deposition is an effective method for making Pt/CA nanocomposites with a high dispersion of Pt. Furthermore, it is possible to control the dispersion of Pt particles through the strength of the interactions between metal precursors and the substrate, metal loading, and the reduction temperature.

Acknowledgment. We gratefully acknowledge the financial support of ICA, the parent company of Aerogel Composite, LLC, in funding this work.

References and Notes

(1) Pekala, R. W. *J. Mater. Sci.* **1989**, *24*, 3221−3227.

(2) Wang, J.; Zhang, S. Q.; Shen, Y. Z.; Guo, S. M.; Attia, B.; Zhou, B.; Lai, Z. Q. *J. Porous Mater*. **2001**, *8*, 167−170.

(3) Petricevic, R.; Glora, M.; Möginger, A.; Fricke, J. *J. Non-Cryst. Solids* **2001**, *285*, 272−276.

(4) Mayer, S. T.; Kong, F. M.; Pekala, R. W.; Kaschmitter, J. L. Organic aerogel microspheres. U.S. Patent 5,908,896, 1999.

(5) Bock, V.; Emmerling, A.; Saliger, R.; Fricke, J. *J. Porous Mater*. **1997**, *4*, 287−294.

(6) Saliger, R.; Fischer, U.; Herta, C.; Fricke, J. *J. Non-Cryst. Solids* **1998**, *225*, 81.

(7) Merzbacher, C. I.; Meier, S. R.; Pierce, J. R.; Korwin, M. L. *J. Non-Cryst. Solids* **2001**, *285*, 210−215.

(8) Yang, K.-L.; Ying, T.-Y.; Yiacoumi, S.; Tsouris, C.; Vittoratos, E. S.; Langmuir. **2001**, *17*(6), 1961−1969.

(9) Haji, S.; Erkey, C. *Ind. Eng. Chem. Res.* **2003**, *42*(26), 6933−6937.

(10) Glora, M.; Wiener, R.; Petricevic, R.; Pröbstle, H.; Fricke, J. *J. Non-Cryst. Solids* **2001**, *285*, 283−287.

(11) Mayer, S. T.; Kaschmitter, J. L.; Pekala, R. W. Carbon aerogel electrodes for direct energy conversion. U.S. Patent 5,601,938, 1997.

(12) Trawczynski, J. *Carbon* **2003**, *41*, 1515−1523.

(13) Erhan Aksoylu, A.; Madalena, M.; Freitas, A.; Fernando, M.; Pereira, R.; Figueiredo, J. L. *Carbon* **2001**, *39*, 175−185.

(14) Auer, E.; Freund, A.; Pietsch, J.; Tacke, T. *Appl. Catal. A* **1998**, *173*, 259−271.

(15) Pajonk, G. M.; Rao, A. V.; Pinto, N.; Ehrburger-Dolle, F.; Bellido Gil, M. In *Preparation of Catalysts VII*; Delmon et al.; Eds. Elsevier Science: Amsterdam, 1998.

(16) Maldonado-Hódar, F. J.; Ferro-Garcia, M. A.; Rivera-Utrilla, J.; Moreno-Castilla, C. *Carbon* **1999**, *37*, 1199.

(17) Fu, R.; Yoshizawa, N.; Fu, R.; Dresselhaus, M. S.; Dresselhaus, G.; Satcher, J. H.; Baumann, T. F. *Langmuir* **2002**, *18*, 10100−10104.

(18) Hammerschmidt, A.; Domke, W. D.; Nolscher, C.; Suchy, P. PEM fuel cell. U.S. Patent 6,010,798, 2000.

(19) Machek, V.; Hanika, J.; Ruzicka, V.; Kunz, J. *Collect. Czech. Chem. Commun.* **1981**, *46*, 3270.

(20) Morley, S. K.; Marr, P. C.; Webb, P. B.; Berry, A. R.; Allison, F. J.; Moldovan, G.; Brown, P. D.; Howdle, S. M. *J. Mater. Chem.* **2002**, *12*, 1898.

(21) Watkins, J. J.; McCarthy, T. J. Method of chemically depositing material onto substrate, U.S. Patent 5,789,027, 1998.

(22) Watkins, J. J.; Blackburn, J. M.; McCarthy, T. J. *Chem. Mater.* **1999**, *11*, 213−215.

(23) Aktary, M.; Lee, C. E.; Xing, Y.; Bergens, S. H.; McDermott, M. T. *Langmuir*, **2000**, *16*, 5837−5840.

(24) Lee, C. E.; Tiege, P. B.; Xing, Y.; Nagendran, J.; Bergens, S. H. *J. Am. Chem. Soc.* **1997**, *119*, 3543−3549.

(25) Xue, Z.; Thridandam, H.; Kaesz, H. D.; Hicks, R. F. *Chem. Mater.* **1992**, *4*, 162−166.

(26) JPCD file No 4802.

(27) Donnet, J. B.; Voet, A. *Carbon Black*, Dekker: New York, 1976.

(28) Anderson, J. R. *Introduction to the Characterization and Testing of Catalysts*; Academic Press: Florida, 1985; Chapter 1.

(29) Wells, P. B. *Appl. Catal.* **1985**, *18*, 259−272.

(30) Kasemo, B.; Törnqvist, E. *Phys. Rev. Lett.* **1980**, *44*, 1555.

(31) Lööf, P.; Kasemo, B.; Andersson, S.; Frestad, A. *J. Catal.* **1991**, *130*, 181.

(32) Holmgren, A.; Andersson, B. *J. Catal.* **1998**, *178*, 14−25.

(33) Ingelsten, H. H.; Skoglundh, M.; Fridell, E. *Appl. Catal. B* **2003**, *41*, 287−300.